Sensitivity Analysis of the Interfrequency Correlation of Synthetic Ground Motions to Pseudodynamic Source Models

Seok Goo Song[*1], Mathieu Causse[2], and Jeff Bayless[3]

Abstract

Given the deficiency of recorded strong ground-motion data, it is important to understand the effects of earthquake rupture processes on near-source ground-motion characteristics and to develop physics-based ground-motion simulation methods for advanced seismic hazard assessments. Recently, the interfrequency correlation of ground motions has become an important element of ground-motion predictions. We investigate the effect of pseudodynamic source models on the interfrequency correlation of ground motions by simulating a number of ground-motion waveforms for the 1994 Northridge, California, earthquake, using the Southern California Earthquake Center Broadband Platform. We find that the cross correlation between earthquake source parameters in pseudodynamic source models significantly affects the interfrequency correlation of ground motions in the frequency around 0.5 Hz, whereas its effect is not visible in the other frequency ranges. Our understanding of the effects of earthquake sources on the characteristics of near-source ground motions, particularly the interfrequency correlation, may help develop advanced physics-based ground-motion simulation methods for advanced seismic hazard and risk assessments.

Cite this article as Song, S. G., M. Causse, and J. Bayless (2020). Sensitivity Analysis of the Interfrequency Correlation of Synthetic Ground Motions to Pseudodynamic Source Models, *Seismol. Res. Lett.* **XX**, 1–13, doi: 10.1785/0220200181.

Introduction

Ground-motion prediction is an important element of the assessment of seismic hazards. In particular, for advanced seismic hazard assessment endeavors, it is important to understand the near-source ground-motion characteristics of large events. Empirical ground-motion prediction equations (GMPEs) have been used extensively to predict ground-motion intensity measures such as the peak ground acceleration (PGA) and pseudospectral acceleration (PSA) (e.g., Abrahamson *et al.*, 2008). However, although ground motions have been recorded worldwide, the quantity of recorded strong ground motions is insufficient to investigate the near-source characteristics, that is, the intensity and variability of ground motions near earthquake fault rupture (Chiou *et al.*, 2008). Recently, physics-based ground-motion simulation approaches, including both dynamic and pseudodynamic earthquake rupture models, have become more popular for evaluating the near-source ground-motion characteristics such as the effect of rupture directivity and fault complexity (e.g., roughness), given the availability of advanced numerical modeling schemes and rapidly growing high-performance computing capabilities (Olsen *et al.*, 2009; Graves *et al.*, 2011; Shi and Day, 2013).

GMPEs predict both the mean and the standard deviation of ground-motion intensity measures such as PGA and PSA, given a set of explanatory seismological parameters (magnitude, distance, site conditions, etc.). Recently, several research groups pioneered a method to investigate the interfrequency (or interperiod) correlation characteristics of ground motions by analyzing recorded ground-motion data (Baker and Cornell, 2006; Baker and Jayaram, 2008; Stafford, 2017; Bayless and Abrahamson, 2019a). The interfrequency correlation characterizes the relative width (in the frequency domain) of the extrema in a ground-motion spectrum. The widths of the peaks and troughs in ground-motion spectra are significant in assessments involving simulated ground motions because the variability in dynamic response analyses can be underestimated if simulated ground motions have an excessively low correlation (Bayless and Abrahamson, 2018).

It would be meaningful to investigate whether physics-based ground-motion simulation models can produce the interfrequency correlation of ground motions, consistent with empirical correlation models, obtained by analyzing recorded ground-motion data. There have been several attempts to understand how well the physics-based ground-motion

1. Earthquake Research Center, Korea Institute of Geoscience and Mineral Resources (KIGAM), Daejeon, Republic of Korea; 2. University of Grenoble Alpes, University of Savoie Mont Blanc, CNRS, IRD, IFSTTAR, University of Gustave Eiffel, ISTerre, Grenoble, France; 3. AECOM, Los Angeles, California, U.S.A.

*Corresponding author: sgsong@kigam.re.kr

simulation models reproduce the mean and the standard deviation of ground-motion intensity measures, produced by empirical GMPEs (Cotton *et al.*, 2013; Causse and Song, 2015; Imtiaz *et al.*, 2015; Vyas *et al.*, 2016; Crempien and Archuleta, 2017; Moschetti *et al.*, 2017; Wirth *et al.*, 2017). Recently, Wang *et al.* (2019) implemented an interfrequency correlation model obtained by analyzing recorded ground-motion data in their physics-based broadband ground-motion simulation platform. In other words, they developed a postprocessing method for their synthetic ground-motion waveforms to mimic the interfrequency correlation structure observed in the empirical model. However, we think that this study is a first attempt to understand the direct link between physics-based ground-motion simulation models and the interfrequency correlation of ground motions.

In this study, we adopted the pseudodynamic source-modeling method, proposed by Song *et al.* (2014) and Song (2016), for physics-based ground-motion simulations, which is implemented at the Southern California Earthquake Center (SCEC) Broadband Platform (BBP). Pseudodynamic source-modeling approaches maintain the computational efficiency of kinematic source-modeling methods but emulate the essential physics of earthquake rupture dynamics by statistically analyzing a number of dynamic rupture models (Guatteri *et al.*, 2004; Graves and Pitarka, 2010; Schmedes *et al.*, 2013; Song *et al.*, 2014). Fayjaloun *et al.* (2019) and Park *et al.* (2020) successfully investigated the effect of the pseudodynamic source models, developed by Song *et al.* (2014) and Song (2016), on the mean and the standard deviation of ground motions. In this study, we investigated the effect of the pseudodynamic source models on the interfrequency correlation of ground motions. We first performed a series of ground-motion simulations for the 1994 Northridge, California, earthquake, using various sets of pseudodynamic source models. Then, we investigated the sensitivity of the interfrequency correlation of the simulated ground motions to those pseudodynamic source models.

Ground-Motion Simulation

For this research, we adopted the BBP developed by the SCEC for synthetic ground-motion simulations (see Data and Resources). Multiple research groups, including both earthquake scientists and engineers, have been involved in the SCEC BBP project (Goulet *et al.*, 2015; Maechling *et al.*, 2015). The BBP has been thoroughly validated against both actual ground motions recorded during past earthquakes and empirical GMPEs (Dreger *et al.*, 2015; Goulet *et al.*, 2015). The latest version of the BBP is released regularly; here, we used version 16.5 (v.16.5), which was released in May 2016. Multiple modeling schemes are provided in the platform; we chose the Song method, which uses pseudodynamic source models, based on the one-point and two-point statistics of earthquake source parameters (Song *et al.*, 2014; Song, 2016). The Song method adopts the Graves and Pitarka (GP) method (Graves and Pitarka, 2010) for the simulation of high-frequency (>1 Hz) ground motions as well as the low-frequency (<1 Hz) seismic-wave propagation. The GP method adopts the Green's function computation method developed by Zhu and Rivera (2002), given a 1D velocity model. In this study, we primarily aimed to investigate the interfrequency correlation of ground motions in the low-frequency range, that is, between 0.1 and 1.0 Hz. Thus, we expect that the interfrequency correlation is mainly affected by the pseudodynamic source models, implemented in ground-motion simulations.

TABLE 1
Fault Geometry of the Northridge Earthquake

Magnitude	**6.73**
Strike, dip, and rake	122°, 40°, and 105°
Length and width	20 and 27 km
H_{Top}*	5 km
Top center (latitude, longitude)†	34.344°, −118.515°
Hypocenter (S_{hyp}‡, D_{hyp}§)	6.0 km, 19.4 km

*Depth to the top of the fault plane.
†Geographical location of the center of the top fault-plane boundary.
‡Hypocenter location in the along-strike direction (distance from the top center of the fault plane).
§Hypocenter location in the along-dip direction (distance from the top center of the fault plane).

The SCEC BBP performed two types of validation (Goulet *et al.*, 2015). The first validation (part A) was against ground-motion data recorded during past earthquakes in North America and Japan. The second (part B) was against empirical GMPEs. Among the part A validation events, we chose the 1994 Northridge, California, earthquake for our study. Detailed information about the fault-plane geometry of the event is given in Table 1 and Figure 1. The Northridge event occurred in a highly populated area and produced well-recorded ground motions, as shown in Figure 1. For the details of the event simulation, we followed the procedure established by the SCEC BBP group (Goulet *et al.*, 2015).

Given the fault geometry defined in Table 1, we prepared three sets of pseudodynamic rupture models for our sensitivity test, as summarized in Table 2. Furthermore, we employed the input source statistics models proposed by Song (2016), which are also summarized in Table 3. The basic set (test set I) in Table 2 is composed of two groups of pseudodynamic source models. One group contains correlated source models, whereas the other contains uncorrelated source models. The core element in the pseudodynamic source models proposed by Song *et al.* (2014) is the cross-correlation structure coupling the earthquake source parameters, such as the slip, rupture velocity, and peak slip velocity. For the group of uncorrelated source models, we simulated the pseudodynamic source

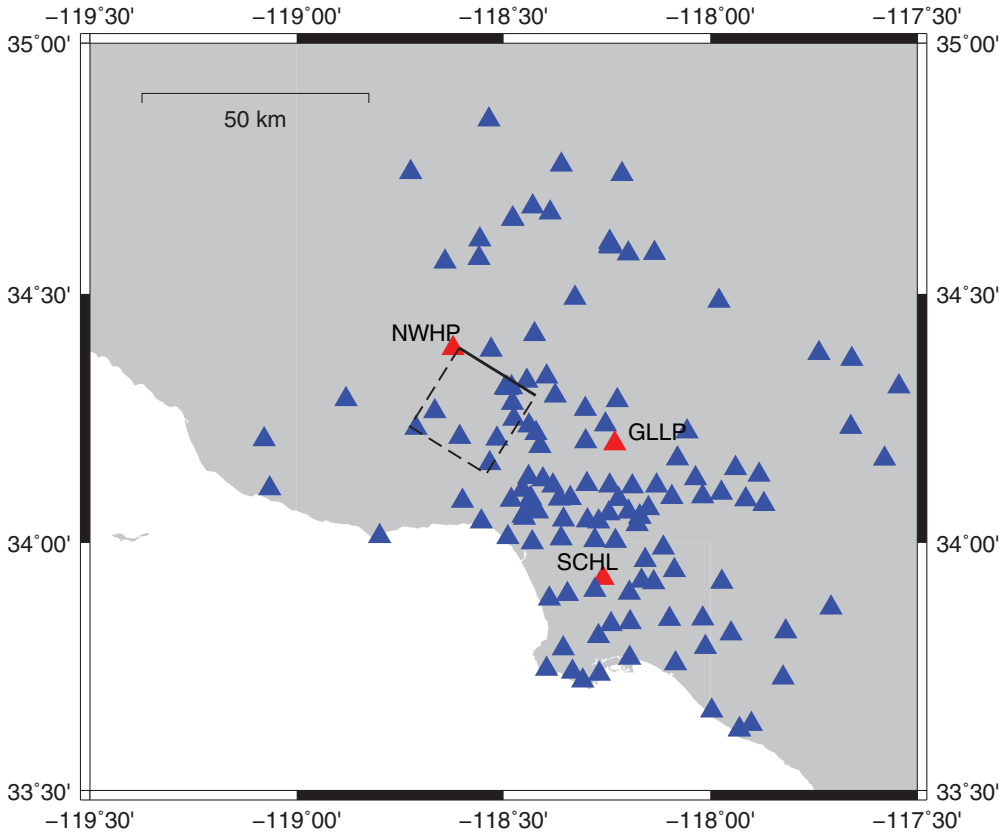

Figure 1. Fault geometry and station locations for the 1994 Northridge, California, earthquake. The black box indicates the ground surface projection of the fault plane; that is, the top of the fault plane is depicted by a solid line, and the rest of the fault plane is delineated with dashed lines. Triangles show the locations of the 133 stations used in the simulation, including the three selected stations in red.

TABLE 2
Three Sets of Model Tests

Test Set	Number of Pseudodynamic Source Models	Description
Test set I (basic)	100 (50 + 50)	50 correlated and 50 uncorrelated source models
Test set II (random hypocenter)	100 (50 + 50)	Same as test set I except that the hypocenter is randomly perturbed
Test set III (stress-drop perturbation)	300 (150 + 150)	150 correlated and 150 uncorrelated source models: the 150 correlated source models are composed of 50 models from test set I, 50 models with a larger stress drop, and 50 models with a smaller stress drop; the 150 uncorrelated source models are produced the same way

models without a cross-correlation structure, as visualized in Figure 2. Several studies have been performed to understand the effects of the cross-correlation structure on near-source ground motions, particularly the mean and the standard deviation of ground-motion intensity measures such as the peak ground velocity and PGA (Fayjaloun *et al.*, 2019; Park *et al.*, 2020).

However, whereas the authors of these studies perturbed each cross-correlation component individually for their sensitivity analysis, we focused on two cases, that is, full cross correlation (correlated) and no cross correlation (uncorrelated) between the earthquake source parameters, as shown in Figure 2. For test set I in Table 2, we simulated 100 pseudodynamic source models, that is, 50 correlated and 50 uncorrelated source models. Figure 3 shows the first three source models among the 50 models in the group of correlated source models, whereas Figure 4 shows the first three for the group of uncorrelated source models. In the correlated source models, the source parameters (such as the slip, rupture velocity, and peak slip velocity) are coupled together according to the cross-correlation structure in Figure 2a. Because the pseudodynamic source models are obtained by stochastic modeling, based on the covariance matrix constructed by the input source statistics models (Song *et al.*, 2014), each source model exhibits unique randomness; nevertheless, we can observe correlations between the source parameters in Figure 3. In contrast, the distributions of the source parameters within the models depicted in Figure 4 display heterogeneity, controlled by the diagonal elements of Figure 2b, but no coupling between the source parameters is expected.

We also prepared two additional sets of pseudodynamic source models, that is, test sets II and III in Table 2, for our sensitivity analysis. In test set II, we randomly perturbed the hypocenter of each source model. In the part A validation, following Goulet *et al.* (2015), the hypocenter was fixed because the validation was performed for real past events. We adopted the same strategy for test set I. However, the hypocenter location

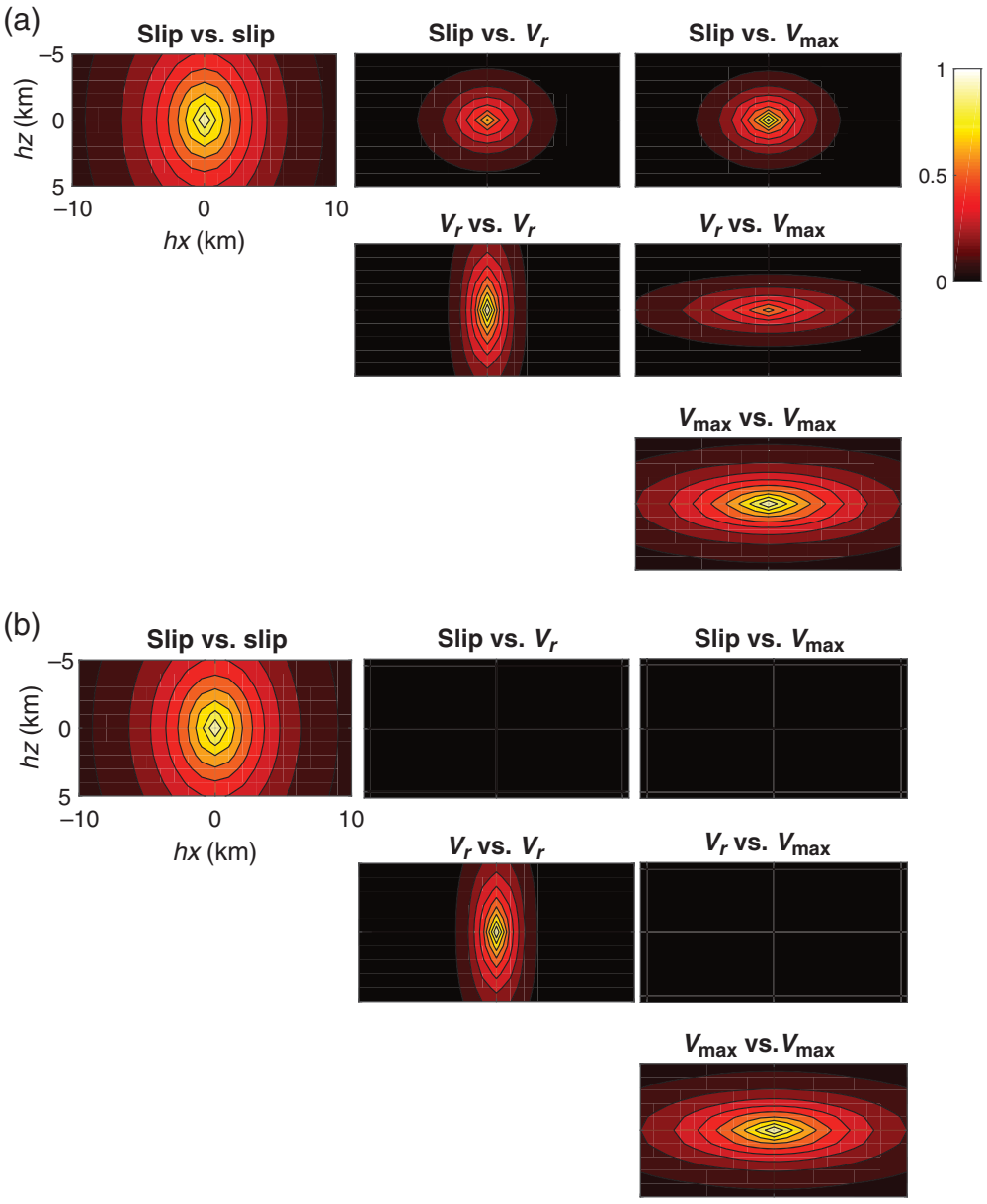

Figure 2. Input correlation model (test set I). (a) Correlated and (b) uncorrelated, that is, without a cross-correlation structure.

may significantly affect the near-source ground-motion characteristics. Therefore, because we aimed to investigate the sensitivity of ground motions to various pseudodynamic source models rather than to validate our pseudodynamic source models against recorded ground-motion data, we decided to test random hypocenter models in test set II as well.

In test set III, we perturbed the stress drop by increasing or decreasing the rupture dimension while holding the seismic moment constant. Because the stress drop directly affects the corner frequency and hence the shape of the Fourier amplitude spectrum (FAS; e.g., Causse and Song, 2015), the stress drop may also affect the interfrequency correlation characteristics of ground motions. The static stress drop is proportional to the ratio of the mean slip to the characteristic rupture dimension ($\widetilde{L}$), as given in the following equation (Kanamori and Anderson, 1975):

$$\Delta\tau \approx \frac{\mu_{\text{slip}}}{\widetilde{L}}. \quad (1)$$

Models with larger stress drops were obtained by decreasing both the rupture length and the width by 30%, whereas models with smaller stress drops were obtained by increasing both the rupture length and the width by 30%. The input source statistics for each model are presented in Table 3. Figures 5 and 6 show one example each of the simulated pseudodynamic source models with larger and smaller stress drops, respectively. In test set III, there are 300 pseudodynamic source models, that is, 150 correlated and 150 uncorrelated models, as indicated in Table 2. The 150 correlated source models contain 50 models with larger stress drops and 50 with smaller stress drops in addition to the 50 correlated source models from test set I.

Using the SCEC BBP (v.16.5), we simulated three-component ground-motion waveforms at the 133 stations illustrated in Figure 1 for each pseudodynamic source model. The Song method adopts a hybrid approach, that is, pseudodynamic low-frequency (<1 Hz; Song, 2016) and stochastic high-frequency (>1 Hz; Graves and Pitarka, 2010) modeling schemes. For a systematic sensitivity analysis of the simulated ground motions with a single representative metric for the ground-motion intensity measures, we adopted the effective amplitude spectrum (EAS), computed with two horizontal-component ground motions as (Bayless and Abrahamson, 2018):

$$\text{EAS}(f) = \sqrt{\frac{1}{2}[\text{FAS}_{HC1}(f)^2 + \text{FAS}_{HC2}(f)^2]}, \quad (2)$$

in which FAS_{HC1} and FAS_{HC2} are the Fourier amplitude spectra of the two orthogonal horizontal components of the three-

TABLE 3
Input Source Statistics Model

Model Parameters	Description	Basic	Larger Stress Drop	Smaller Stress Drop
One-point statistics				
μ_{slip}	Mean slip (cm)	78.36	159.08	46.50
μ_{V_r}	Mean rupture velocity (km/s)	3.27	3.30	3.26
$\mu_{V_{max}}$	Mean peak slip velocity (cm/s)	114.93	158.24	97.84
σ_{slip}	Standard deviation of slip (cm)	45.15	90.83	27.11
σ_{V_r}	Standard deviation of rupture velocity (km/s)	1.08	1.17	1.04
$\sigma_{V_{max}}$	Standard deviation of peak slip velocity (cm/s)	89.00	125.64	74.54
Two-point statistics				
a_x	Correlation length in the along-strike direction (km) (slip vs. slip, slip vs. V_r, slip vs. V_{max}, V_r vs. V_r, V_r vs. V_{max}, and V_{max} vs. V_{max})	$\begin{pmatrix} 3.9 & 2.7 & 2.4 \\ & 1.3 & 5.6 \\ & & 6.2 \end{pmatrix}$	$\begin{pmatrix} 3.5 & 2.6 & 1.7 \\ & 1.3 & 4.9 \\ & & 4.7 \end{pmatrix}$	$\begin{pmatrix} 4.1 & 2.7 & 2.7 \\ & 1.3 & 5.9 \\ & & 7.0 \end{pmatrix}$
a_z	Correlation length in the along-dip direction (km) (slip vs. slip, slip vs. V_r, slip vs. V_{max}, V_r vs. V_r, V_r vs. V_{max}, and V_{max} vs. V_{max})	$\begin{pmatrix} 5.6 & 2.0 & 1.6 \\ & 3.6 & 1.4 \\ & & 1.9 \end{pmatrix}$	$\begin{pmatrix} 13.3 & 4.0 & 3.9 \\ & 4.2 & 1.9 \\ & & 2.4 \end{pmatrix}$	$\begin{pmatrix} 4.0 & 1.5 & 1.1 \\ & 3.4 & 1.3 \\ & & 1.8 \end{pmatrix}$
ρ_{max}	Maximum correlation coefficient (slip vs. V_r, slip vs. V_{max}, and V_r vs. V_{max})	$\begin{pmatrix} 1 & 0.72 & 0.94 \\ & 1 & 0.64 \\ & & 1 \end{pmatrix}$	$\begin{pmatrix} 1 & 0.81 & 0.89 \\ & 1 & 0.69 \\ & & 1 \end{pmatrix}$	$\begin{pmatrix} 1 & 0.68 & 0.96 \\ & 1 & 0.62 \\ & & 1 \end{pmatrix}$

component waveforms and f is the frequency in Hertz. The EAS is independent of the orientation of the instrument. Using the average power of the two horizontal components (equation 2) leads to an amplitude spectrum that is compatible with the application of random vibration theory to convert the Fourier spectra into response spectra. The EAS is smoothed using the $\log_{10}$-scale smoothing window of Konno and Ohmachi (1998) with the smoothing parameters described by Kottke *et al.* (2018).

Figure 7 shows examples of the EAS for the three selected stations plotted in red in Figure 1. For the near-source station (NWHP, $R_{rup} = 5.4$ km), the low- and high-frequency EAS do not differ considerably, but for the other two stations (GLLP, $R_{rup} = 21.5$ km; SCHL, $R_{rup} = 40.4$ km), the two frequency bands, that is, the low-frequency (<1 Hz) and high-frequency (>1 Hz) bands, show distinctive EAS patterns. Because we used the aforementioned hybrid approach, the low- and high-frequency ground motions may not behave consistently for all rupture scenarios and station locations. This issue may need to be investigated further for all hybrid ground-motion simulation methods offered by the SCEC BBP. In this study, we aimed predominantly to analyze low-frequency (<1 Hz) ground motions, which are affected by the cross-correlation structure of the input pseudodynamic source models, for the sensitivity analysis of interfrequency correlations. We also added the mean and the standard deviation values predicted by the empirical model (Bayless and Abrahamson, 2019b) to the figure for comparison purposes. The empirical model used in the study will be discussed in more details in the next section.

Correlation Analysis

Bayless and Abrahamson (2019a,b) developed both the interfrequency correlation model and the GMPE using the Next Generation Attenuation-West2 (Ancheta *et al.*, 2014) database, which includes shallow crustal earthquakes in active tectonic regions. Their models adopt the EAS, which is based on the FAS, in equation (2) as ground-motion intensity measure. Bayless and Abrahamson (2019b) clearly described the benefit of using the EAS than response spectra in their article. We adopted their EAS-based GMPE and interfrequency correlation model to compare with our synthetics because the Fourier spectra are more closely related to the physics-based simulations. Their empirical models also provide individual residual components for more detailed comparison. Residuals from empirical GMPEs are typically partitioned into between-event residual (δB), and within-event residuals (δW), following the notation of Al Atik *et al.* (2010). For large numbers of recordings per earthquake, the between-event residual is approximately the average difference in logarithmic space between the observed intensity measure (IM) from a specific earthquake and the IM predicted by the GMPE. The within-event residual (δW) is the difference between the IM at a specific site for a given earthquake and the median IM predicted by the GMPE plus δB. By accounting for repeatable site effects, δW can further be partitioned into a site-to-site residual (δS2S) and the within-site residual (δWS). More detailed description about the residual partitioning, including the mathematical description of the interfrequency correlation (both between and within event), is provided in Bayless and Abrahamson (2018).

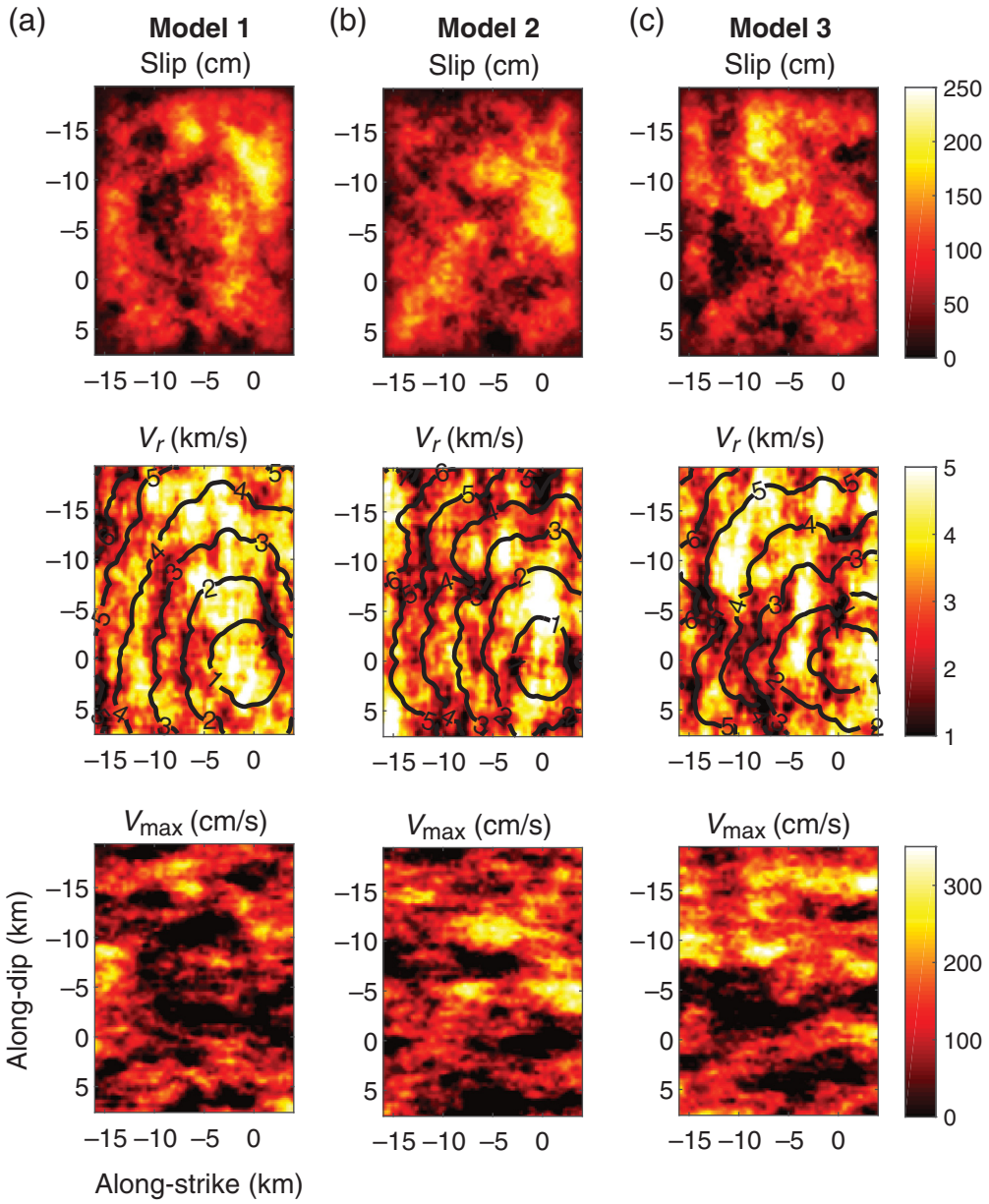

Figure 3. (a–c) Three correlated pseudodynamic source models. The contour lines in the middle panels indicate rupture-time distributions. The hypocenter is located at the bottom-right corner of the rupture area.

Figure 8 shows the mean residuals on a natural logarithmic scale between the simulated EAS and the EAS predicted by the empirical GMPE (Bayless and Abrahamson, 2019b) for both the correlated and the uncorrelated models in test set I. We observed that the mean of the synthetic EAS underpredicts the mean of the GMPE at the low frequency, whereas the mean of the former overpredicts that of the latter at the high frequency. At the low frequency, the correlated models produce slightly higher EAS, as was also observed in previous studies (Song *et al.*, 2014; Song, 2016; Fayjaloun *et al.*, 2019; Park *et al.*, 2020). Because we compared synthetic ground motions produced by simulating a specific earthquake, that is, the Northridge event, and because we constructed the mean of the GMPE using recorded ground motions from various events worldwide, the bias we observe in Figure 8 may be reasonable and may be considered part of the between-event variability (Al Atik *et al.*, 2010). In addition, we aimed to investigate mainly the relative sensitivity of the interfrequency correlation of our synthetic ground motions in this study rather than to reproduce the absolute level of ground-motion intensities constrained by empirical GMPEs.

The variability (e.g., standard deviation) of ground motions is an important consideration in ground-motion prediction (Abrahamson *et al.*, 2008; Cotton *et al.*, 2013; Causse and Song, 2015; Imtiaz *et al.*, 2015; Vyas *et al.*, 2016; Crempien and Archuleta, 2017; Withers *et al.*, 2019a,b). Figure 9 shows the standard deviations for both the between-event and the within-event components of the EAS residuals from the three sets of model tests. The between-event term is calculated from various realizations of the source within each test set. First, little difference is noted between the ground motions obtained from the correlated and uncorrelated pseudodynamic source models. In other words, the cross correlations between the earthquake source parameters in Figure 2 do not significantly affect both the between-event and the within-event standard deviations in our simulations. Crempien and Archuleta (2017) found that the longer correlation (i.e., autocorrelation) of earthquake slip increases both the between- and within-event standard deviations of ground motions. The cross correlation of pseudodynamic source models does not seem to play a significant role in determining the standard deviation in our simulations but may need to be further investigated in subsequent studies to confirm its behavior.

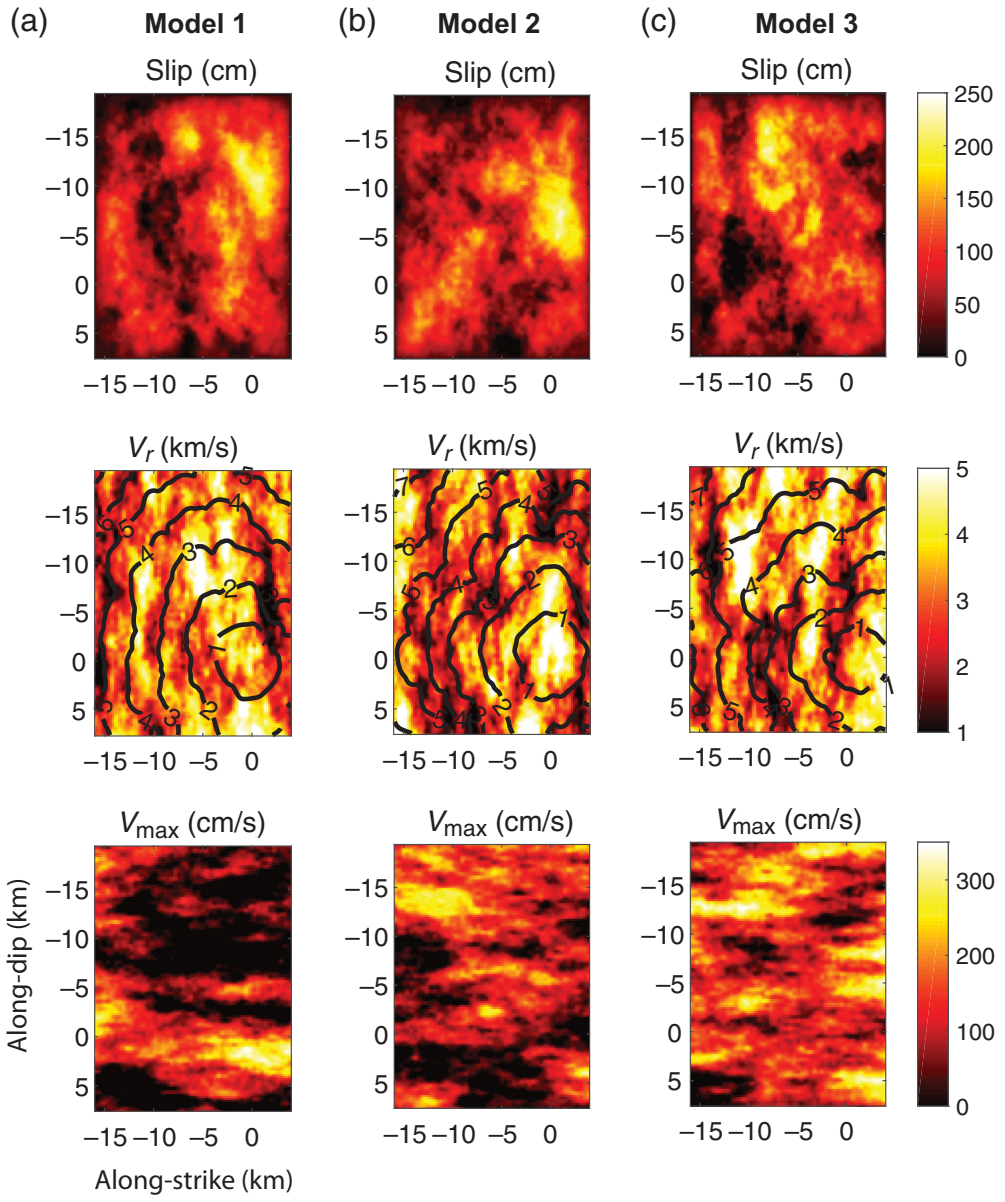

Figure 4. (a–c) Three uncorrelated pseudodynamic source models. The contour lines in the middle panels indicate rupture time distributions. The hypocenter is located at the bottom-right corner of the rupture area.

The between-event standard deviation for test set II (random hypocenter) is much larger than that for the other two test sets. Because test set II introduces randomly located hypocenters, this discrepancy implies that randomizing the hypocenter has a greater effect on the between-event variability than does the stress-drop perturbation. It is also noticeable that the random hypocenter models reduce the within-event standard deviation significantly as shown in Figure 9b. We also compared them with the standard deviations from the empirical GMPE (Bayless and Abrahamson, 2019b) as indicated in black lines. Regarding the between-event standard deviation, the empirical model is consistent with the synthetic ground motions with the random hypocenter models. Regarding the within-event standard deviation, in general synthetic ground motions produce larger values. For the random hypocenter model in Figure 9b, the difference is minimized. However, if we consider only the within-site (δWS) standard deviation without the between-site (δS2S) term because the site effect was not included in our simulations, the synthetics still produce larger standard deviations. We restricted our analysis to the low frequency below 1 Hz, although we show the results up to 10 Hz for reference in the figure.

The main goal of this study was to investigate the effect of cross correlations between earthquake source parameters, such as the slip, rupture velocity, and peak slip velocity, in pseudodynamic source models on the interfrequency correlation of ground motions. Figure 10 shows the between-event interfrequency correlations of the synthetic EAS for the three sets of model tests in the low-frequency band (0.1–1.0 Hz) with those from an empirical model (Bayless and Abrahamson, 2019a). Interestingly, the between-event interfrequency correlations for the fixed-hypocenter models decay much faster than those for the empirical model as the frequency deviates from the reference frequencies (0.2, 0.3, 0.4, 0.5, and 1.0 Hz), whereas the random hypocenter models produce interfrequency correlations that are compatible with those from the empirical model. More remarkably, we found distinctive features between the correlated and uncorrelated models at approximately 0.5 Hz (2 s) when the reference frequencies were 0.4 Hz (test set II) or 0.5 Hz (test sets I and III): the correlated source models (in red) produced higher interfrequency correlations than the uncorrelated source models (in blue) for all three test sets at approximately 0.5 Hz, although the difference was not significant at the other reference frequencies. In

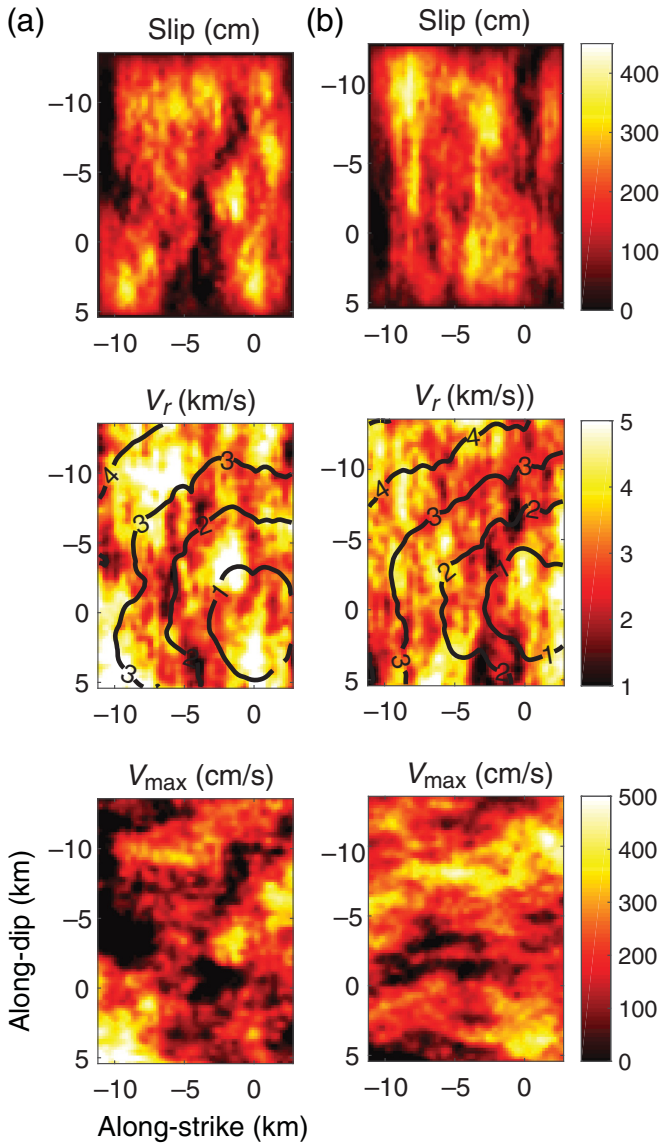

Figure 5. Pseudodynamic source models with a larger stress drop. (a) Correlated and (b) uncorrelated. The contour lines in the middle panels indicate rupture-time distributions. The hypocenter is located at the bottom-right corner of the rupture area.

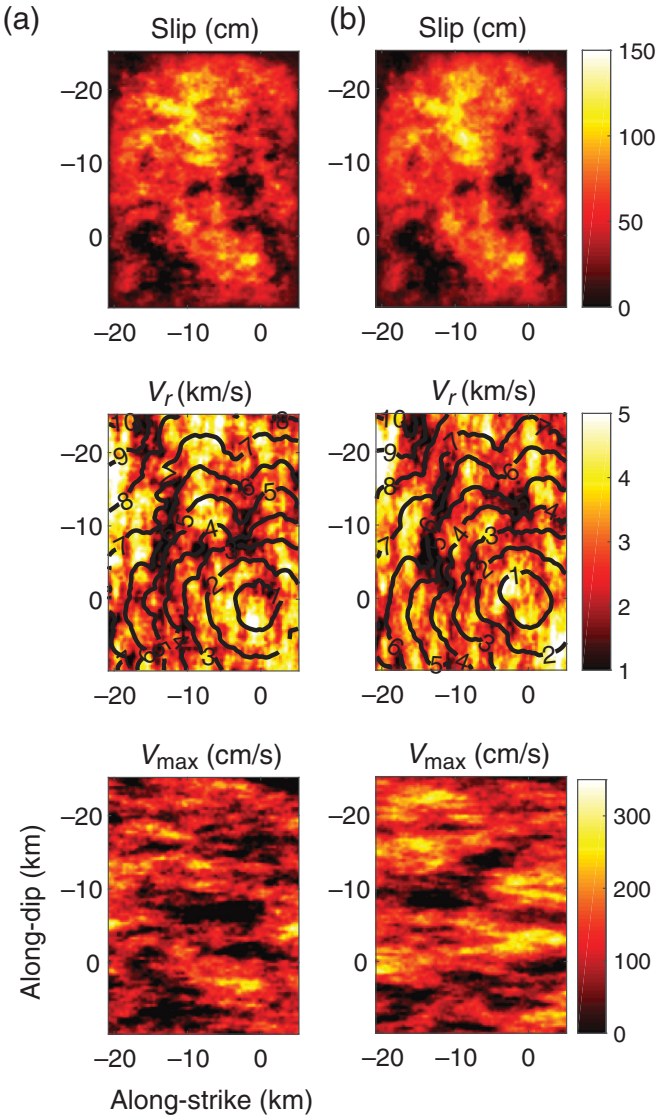

Figure 6. Pseudodynamic source models with a smaller stress drop. (a) Correlated and (b) uncorrelated. The contour lines in the middle panels indicate rupture-time distributions. The hypocenter is located at the bottom-right corner of the rupture area.

this analysis, we focus more on the correlation near each reference frequency, that is, initial decay pattern from each reference frequency. Thus, we show correlations only between 0.6 and 1.0 in Figure 10. The correlation at the far distance in the spectral domain may need to be analyzed further in subsequent studies. This observation, however, may imply that the cross correlation between earthquake source parameters in pseudodynamic source models affects the initial decay pattern of the interfrequency correlation of ground motions in a certain frequency range, as depicted with solid red and blue traces in Figure 10.

Within-event residuals represent the variability in the path effects and directivity effects for a given event at various stations. Figure 11 indicates that the interfrequency correlations of simulated ground motions systematically exceed those of the empirical model. We do not observe significant differences between correlated and uncorrelated pseudodynamic source models. It is not clear yet why the synthetic ground motions produce broader interfrequency correlation structure than the empirical model. Based on Bayless and Abrahamson (2018), the fully stochastic ground-motion simulation methods (e.g., Atkinson and Assatourians, 2015) produce the within-event interfrequency correlations compatible with the empirical model (Bayless and Abrahamson, 2018, their fig. 10b), whereas the physics-based ground-motion simulation methods produce the correlations, which are broader than the empirical model (Bayless and

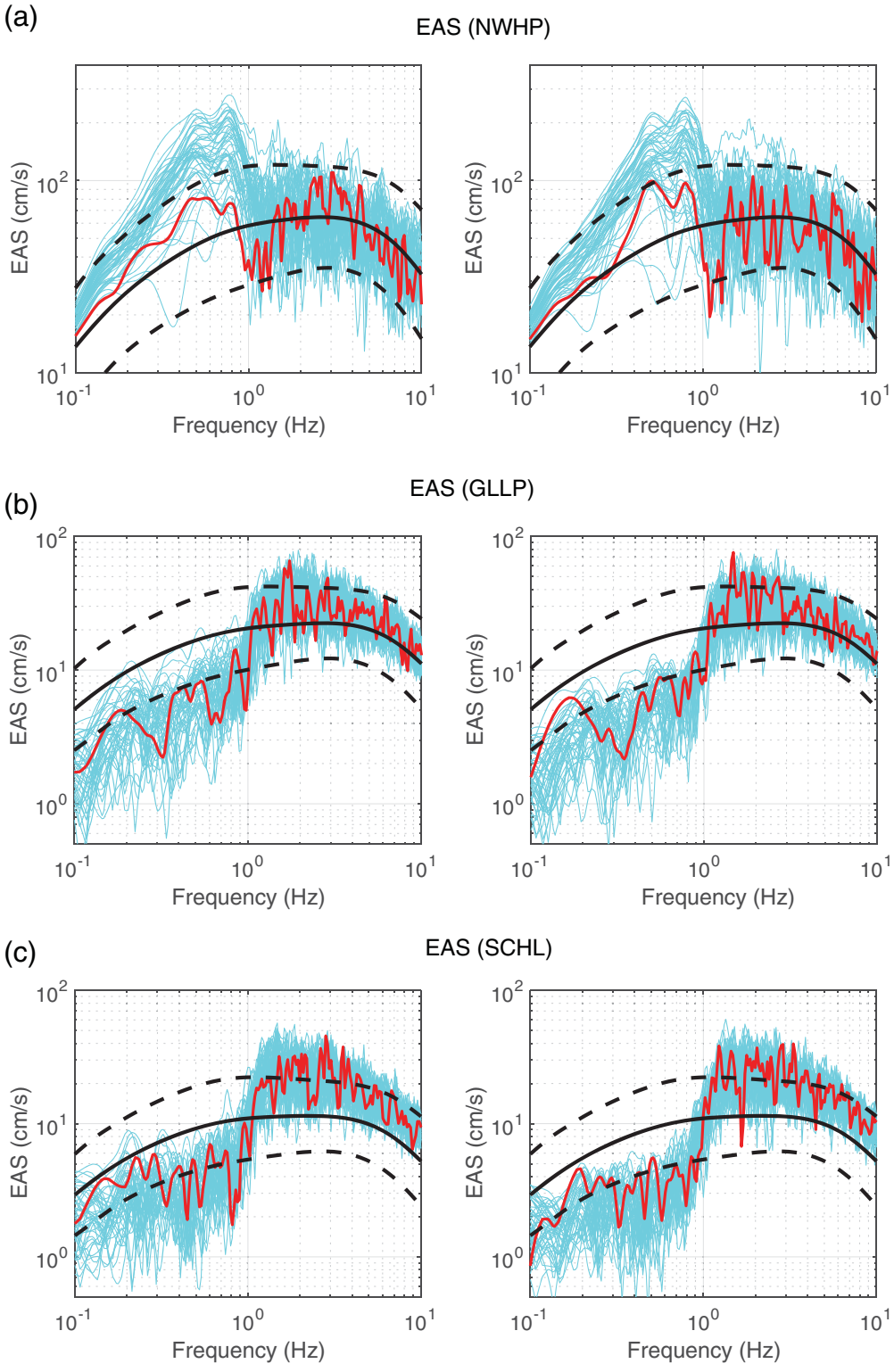

Figure 7. Effective amplitude spectra (EAS) obtained from test set I for the stations (a) NWHP, (b) GLLP, and (c) SCHL plotted in red in Figure 1. Fifty EAS values are plotted in cyan in each panel. The 50th EAS is added in red as an example. (left panel) EAS obtained from the correlated pseudodynamic source models; (right panel) EAS obtained from the uncorrelated source models. Both mean and standard deviation from the empirical ground-motion prediction equation (GMPE) model (Bayless and Abrahamson, 2019b) are presented for comparison purposes.

Abrahamson, 2018, their figs. 11b–14b). It is still puzzling why the physics-based methods, which more explicitly handle wave-propagation effects such as directivity, produce the within-event correlations inconsistent with the empirical model. Although we aim to focus more on the effect of earthquake source on the interfrequency correlations, that is, between-event, the inconsistency observed in the within-event correlation may need to be investigated further in subsequent studies.

Discussion

In Figure 10, the cross correlation in the pseudodynamic source models affects the between-event interfrequency correlation of ground motions in a specific frequency range, that is, approximately 0.5 Hz. However, it is not yet clear why the frequency range centered at approximately 0.5 Hz is strongly affected by the cross correlation of pseudodynamic source models for the Northridge, California, earthquake. It is also surprising that there are almost no differences in the other frequency ranges. This phenomenon may be linked to the magnitude of the simulated event or the event type. The reason may become clearer if we perform more sensitivity analyses over a wide range of magnitudes and event types in subsequent studies. Moreover, the number and positions of stations used in the analyses may also affect the outcomes. Test sets II and III clearly indicate that the interfrequency correlation can be affected by randomized hypocenter locations and stress-drop perturbations more

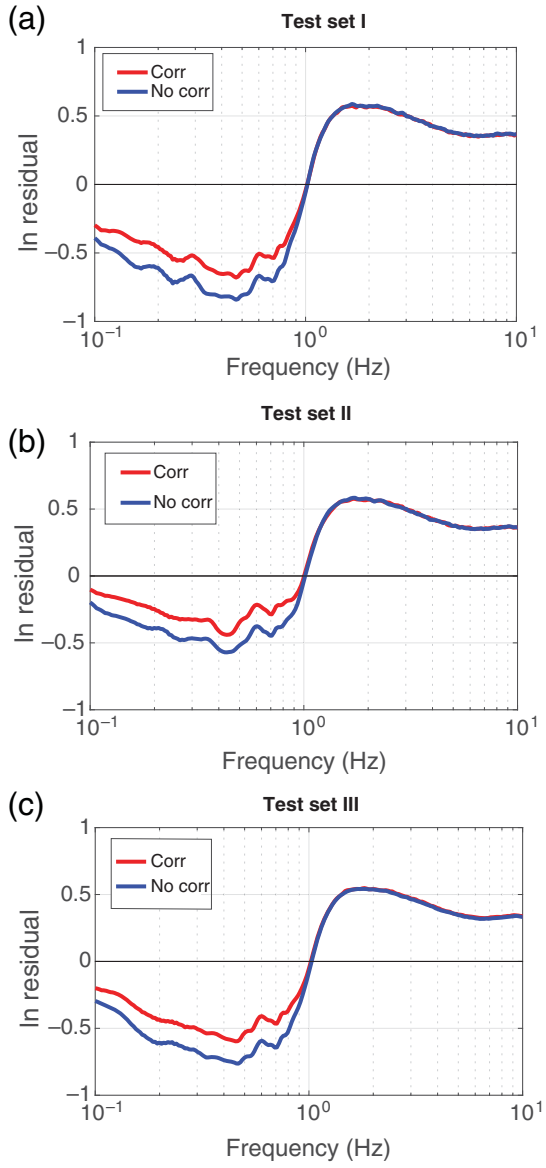

Figure 8. Mean residuals between the simulated EAS and those predicted by the empirical GMPE (Bayless and Abrahamson, 2019b). (a) Test set I (basic), (b) test set II (random hypocenter), and (c) test set III (stress-drop perturbation). Corr, correlation.

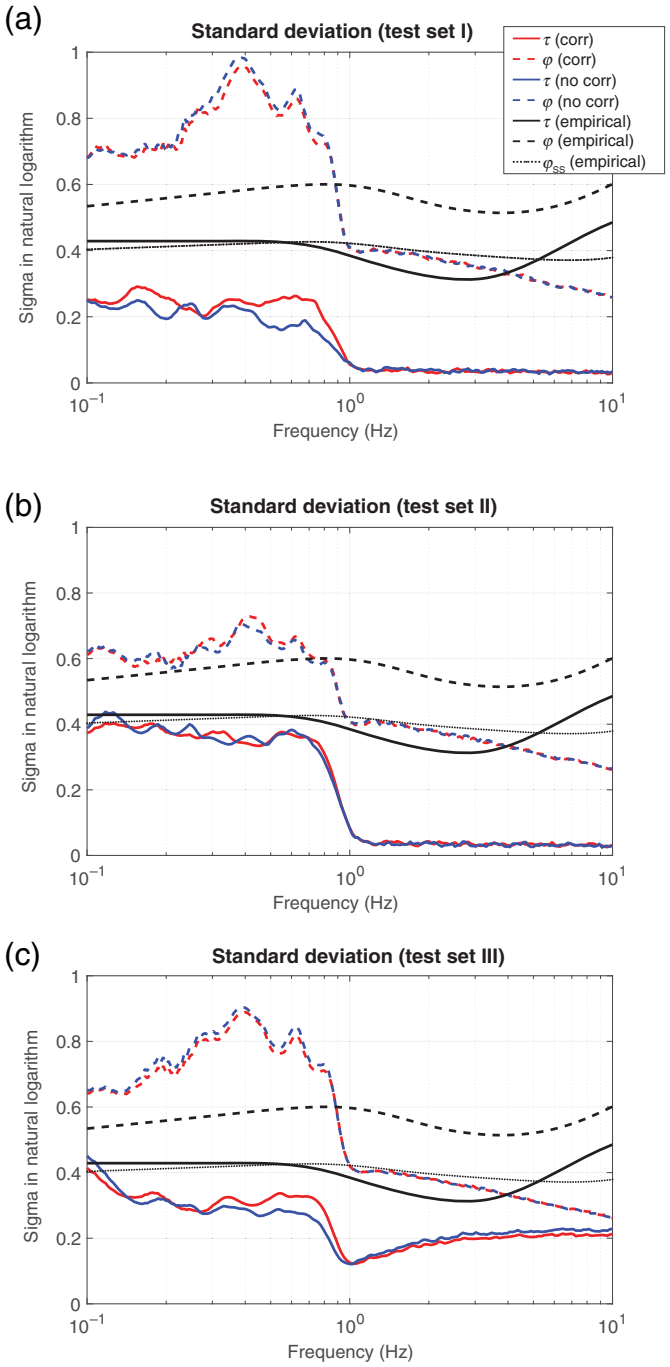

Figure 9. Standard deviations (τ: between-event, φ: within-event, and φ_{SS}: within-site) of the EAS residuals in (a) test set I (basic), (b) test set II (random hypocenter), and (c) test set III (stress-drop perturbation). For the within-event standard deviation from the empirical model, both the within-event (i.e., within-site and between-site terms) and only the within-site standard deviations are presented for the comparison purposes.

significantly than by input source statistics perturbations, as shown in Table 3. Hence, we need to carefully consider these source parameters, such as the hypocenter and stress drop, even when we focus on investigating the effects of the detailed input source statistics in Table 3 on the characteristics of ground motions. Finally, our sensitivity analyses clearly indicate that the cross-correlation structure in the pseudodynamic source models affects the interfrequency correlation more significantly than the standard deviation of the ground motions. We may also employ the empirical interfrequency correlation model (Bayless and Abrahamson, 2019a) to constrain the cross-correlation structure of pseudodynamic source models.

There have been several attempts to investigate the effects of pseudodynamic source models on the mean and standard deviation of ground motions (Song *et al.*, 2014; Song, 2016; Fayjaloun *et al.*, 2019; Park *et al.*, 2020). However, this study

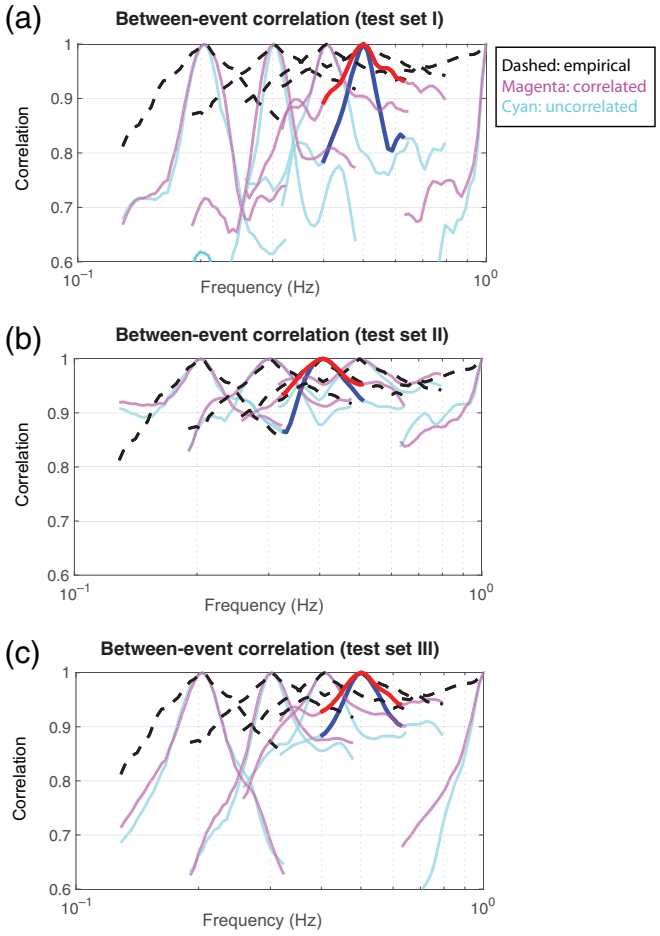

Figure 10. Interfrequency correlations (between event) with five reference frequencies (0.2, 0.3, 0.4, 0.5, and 1.0 Hz) in (a) test set I (basic), (b) test set II (random hypocenter), and (c) test set III (stress-drop perturbation). The initial decay patterns of both correlated and uncorrelated source models from the reference frequencies, i.e., 0.5 Hz for (a) and (c), and 0.4 Hz for (b), are emphasized with red and blues lines, respectively.

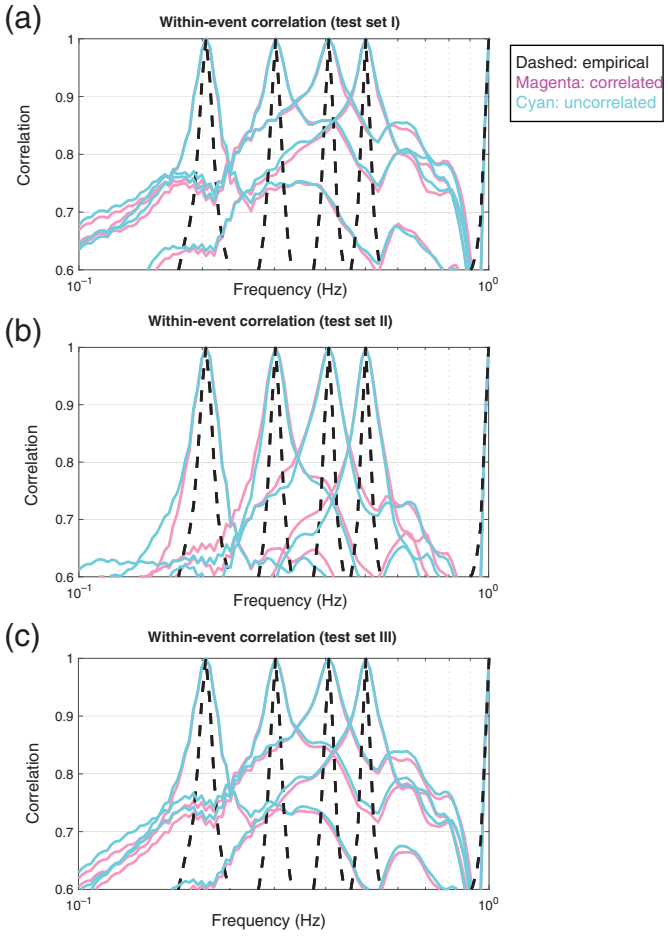

Figure 11. Interfrequency correlations (within-event) with five reference frequencies (0.2, 0.3, 0.4, 0.5, and 1.0 Hz) in (a) test set I (basic), (b) test set II (random hypocenter), and (c) test set III (stress-drop perturbation).

is the first attempt to investigate the effect of pseudodynamic source models on the interfrequency correlation of ground motions. Interestingly, we found that the cross-correlation structure, which is a core element of the pseudodynamic source-modeling approach proposed by Song *et al.* (2014), may significantly affect the interfrequency correlation of ground motions, at least in a specific frequency range. Nevertheless, we may need more comprehensive sensitivity analyses to understand the link between pseudodynamic source models and the interfrequency correlation of ground motions in greater detail. However, we believe that this pilot study already shows the potential of physics-based ground-motion simulation methods provided by the SCEC BBP for studying the interfrequency correlation characteristics of ground motions.

Conclusions

In this study, we investigated the effect of pseudodynamic source models, particularly their cross-correlation structure between earthquake source parameters, on the interfrequency correlation of ground motions by simulating a number of ground motions for the 1994 Northridge, California, earthquake using the SCEC BBP. We found that the cross correlation of pseudodynamic source models significantly affects the between-event interfrequency correlation at a specific frequency range (at approximately 0.5 Hz), although the effect on the standard deviation of ground motions is not significant. It is important to understand the interfrequency correlation characteristics of ground motions in ground-motion predictions. This type of study may help to understand the relation between physics-based earthquake source models and the interfrequency correlation of ground motions and consequently to develop physics-based ground-motion simulation methods for advanced seismic hazard and risk assessments.

Data and Resources

We simulated synthetic three-component ground-motion waveforms using the Southern California Earthquake Center (SCEC) Broadband Platform (BBP) (version 16.5), which is available online (http://scec.usc.edu/scecpedia/Broadband_Platform, last accessed April 2020). The stand-alone version of the pseudodynamic rupture model generator, used in the study, is also available online (http://www.github.com/sgsong1017/SongRMG, last accessed July 2020).

Acknowledgments

The authors appreciate the editor's and three anonymous reviewers' comments, which helped improve the article significantly. The authors would like to thank F. Silva, P. Maechling, C. Goulet, and R. W. Graves for their kind technical and scientific support regarding the Southern California Earthquake Center (SCEC) Broadband Platform (BBP). This study was supported by a See-At Project funded by the Korea Meteorological Administration (KMA) (KMI2018-01810) and by a Basic Research Project of the Korea Institute of Geoscience and Mineral Resources (KIGAM), funded by the Ministry of Science and ICT (MSIT, Korea) (GP2020-027).

References

Abrahamson, N., G. Atkinson, D. Boore, Y. Bozorgnia, K. Campbell, B. Chiou, I. M. Idriss, W. Silva, and R. Youngs (2008). Comparisons of the NGA ground-motion relations, *Earthq. Spectra* **24,** 45–66.

Al Atik, L., N. Abrahamson, J. J. Bommer, F. Scherbaum, F. Cotton, and N. Kuehn (2010). The variability of ground-motion prediction models and its components, *Seismol. Res. Lett.* **81,** 794–801.

Ancheta, T. D., R. B. Darragh, J. P. Stewart, E. Seyhan, W. J. Silva, B. S.-J. Chiou, K. E. Wooddell, R. W. Graves, A. R. Kottke, D. M. Boore, *et al.* (2014). NGA-West2 database, *Earthq. Spectra* **30,** 989–1005.

Atkinson, G. M., and K. Assatourians (2015). Implementation and validation of EXSIM (a stochastic finite-fault ground-motion simulation algorithm) on the SCEC Broadband Platform, *Seismol. Res. Lett.* **86,** 48–60.

Baker, J. W., and C. A. Cornell (2006). Correlation of response spectral values for multicomponent ground motions, *Bull. Seismol. Soc. Am.* **96,** 215–227.

Baker, J. W., and N. Jayaram (2008). Correlation of spectral acceleration values from NGA ground motion models, *Earthq. Spectra* **24,** 299–317.

Bayless, J., and N. A. Abrahamson (2018). Evaluation of the interperiod correlation of ground-motion simulations, *Bull. Seismol. Soc. Am.* **108,** 3413–3430.

Bayless, J., and N. A. Abrahamson (2019a). An empirical model for the interfrequency correlation of epsilon for Fourier amplitude spectra, *Bull. Seismol. Soc. Am.* **109,** 1058–1070.

Bayless, J., and N. A. Abrahamson (2019b). Summary of the BA18 ground-motion model for Fourier amplitude spectra for crustal earthquakes in California, *Bull. Seismol. Soc. Am.* **109,** 2088–2105.

Causse, M., and S. G. Song (2015). Are stress drop and rupture velocity of earthquakes independent? Insight from observed ground motion variability, *Geophys. Res. Lett.* **42,** 7383–7389.

Chiou, B., R. Darragh, N. Gregor, and W. Silva (2008). NGA project strong-motion database, *Earthq. Spectra* **24,** 23–44.

Cotton, F., R. Archuleta, and M. Causse (2013). What is sigma of the stress drop? *Seismol. Res. Lett.* **84,** 42–48.

Crempien, J. G. F., and R. J. Archuleta (2017). Within-event and between-events ground motion variability from earthquake rupture scenarios, *Pure Appl. Geophys.* **174,** 3451–3465.

Dreger, D. S., G. C. Beroza, S. M. Day, C. A. Goulet, T. H. Jordan, P. A. Spudich, and J. P. Stewart (2015). Validation of the SCEC Broadband Platform V14.3 simulation methods using pseudospectral acceleration data, *Seismol. Res. Lett.* **86,** 39–47.

Fayjaloun, R., M. Causse, C. Cornou, C. Voisin, and S. G. Song (2019). Sensitivity of high-frequency ground motion to kinematic source parameters, *Pure Appl. Geophys.* **177,** 1947–1967, doi: 10.1007/s00024-019-02195-3.

Goulet, C. A., N. A. Abrahamson, P. G. Somerville, and K. E. Wooddell (2015). The SCEC Broadband Platform validation exercise: Methodology for code validation in the context of seismic-hazard analyses, *Seismol. Res. Lett.* **86,** 17–26.

Graves, R., T. H. Jordan, S. Callaghan, E. Deelman, E. Field, G. Juve, C. Kesselman, P. Maechling, G. Mehta, K. Milner, *et al.* (2011). Cybershake: A physics-based seismic hazard model for southern California, *Pure Appl. Geophys.* **168,** 367–381.

Graves, R. W., and A. Pitarka (2010). Broadband ground-motion simulation using a hybrid approach, *Bull. Seismol. Soc. Am.* **100,** 2095–2123.

Guatteri, M., P. M. Mai, and G. C. Beroza (2004). A pseudo-dynamic approximation to dynamic rupture models for strong ground motion prediction, *Bull. Seismol. Soc. Am.* **94,** 2051–2063.

Imtiaz, A., M. Causse, E. Chaljub, and F. Cotton (2015). Is ground-motion variability distance dependent? Insight from finite-source rupture simulations, *Bull. Seismol. Soc. Am.* **105,** 950–962.

Kanamori, H., and D. L. Anderson (1975). Theoretical basis of some empirical relations in seismology, *Bull. Seismol. Soc. Am.* **65,** 1073–1095.

Konno, K., and T. Ohmachi (1998). Ground-motion characteristics estimated from spectral ratio between horizontal and vertical components of microtremor, *Bull. Seismol. Soc. Am.* **88,** 228–241.

Kottke, A., E. Rathje, D. M. Boore, E. Thompson, J. Hollenback, N. Kuehn, C. A. Goulet, N. A. Abrahamson, Y. Bozorgnia, and A. D. Kiureghian (2018). *Selection of Random Vibration Procedures for the NGA East Project*, *PEER Rept. 2018/05*, Pacific Earthquake Engineering Research Center, University of California, Berkeley, California.

Maechling, P. J., F. Silva, S. Callaghan, and T. H. Jordan (2015). SCEC Broadband Platform: System architecture and software implementation, *Seismol. Res. Lett.* **86,** 27–38.

Moschetti, M. P., S. Hartzell, L. Ramírez-Guzmán, A. D. Frankel, S. J. Angster, and W. J. Stephenson (2017). 3D ground-motion simulations of M_w 7 earthquakes on the Salt Lake City segment of the Wasatch fault zone: Variability of long-period ($T \geq 1$ s) ground motions and sensitivity to kinematic rupture parameters, *Bull. Seismol. Soc. Am.* **107,** 1704–1723.

Olsen, K. B., S. M. Day, L. A. Dalguer, J. Mayhew, Y. Cui, J. Zhu, V. M. Cruz-Atienza, D. Roten, P. Maechling, T. H. Jordan, *et al.* (2009). ShakeOut-D: Ground motion estimates using an ensemble of large earthquakes on the southern San Andreas fault with spontaneous rupture propagation, *Geophys. Res. Lett.* **36,** L04303, 1–6.

Park, D., S. G. Song, and J. Rhie (2020). Sensitivity analysis of near-source ground motions to pseudo-dynamic source models derived

with 1-point and 2-point statistics of earthquake source parameters, *J. Seismol.* doi: 10.1007/s10950-020-09905-8.

Schmedes, J., R. J. Archuleta, and D. Lavallée (2013). A kinematic rupture model generator incorporating spatial interdependency of earthquake source parameters, *Geophys. J. Int.* **192,** 1116–1131.

Shi, Z., and S. M. Day (2013). Rupture dynamics and ground motion from 3-D rough-fault simulations, *J. Geophys. Res.* **118,** 1122–1141.

Song, S. G. (2016). Developing a generalized pseudo-dynamic source model of M_w 6.5–7.0 to simulate strong ground motions, *Geophys. J. Int.* **204,** 1254–1265.

Song, S. G., L. A. Dalguer, and P. M. Mai (2014). Pseudo-dynamic source modelling with 1-point and 2-point statistics of earthquake source parameters, *Geophys. J. Int.* **196,** 1770–1786.

Stafford, P. J. (2017). Interfrequency correlations among Fourier spectral ordinates and implications for stochastic ground-motion simulation, *Bull. Seismol. Soc. Am.* **107,** 2774–2791.

Vyas, J. C., P. M. Mai, and M. Galis (2016). Distance and azimuthal dependence of ground-motion variability for unilateral strike-slip ruptures, *Bull. Seismol. Soc. Am.* **106,** 1584–1599.

Wang, N., R. Takedatsu, K. B. Olsen, and S. M. Day (2019). Broadband ground-motion simulation with interfrequency correlations, *Bull. Seismol. Soc. Am.* **109,** 2437–2446.

Wirth, E. A., A. D. Frankel, and J. E. Vidale (2017). Evaluating a kinematic method for generating broadband ground motions for great subduction zone earthquakes: Application to the 2003 M_w 8.3 Tokachi-Oki earthquake, *Bull. Seismol. Soc. Am.* **107,** 1737–1753.

Withers, K. W., K. B. Olsen, Z. Shi, and S. M. Day (2019a). Ground motion and intraevent variability from 3D deterministic broadband (0–7.5 Hz) simulations along a non-planar strike-slip fault, *Bull. Seismol. Soc. Am.* **109,** 212–228.

Withers, K. W., K. B. Olsen, Z. Shi, and S. M. Day (2019b). Validation of deterministic broadband ground motion and variability from dynamic rupture simulations of buried thrust earthquakes, *Bull. Seismol. Soc. Am.* **109,** 229–250.

Zhu, L. P., and L. A. Rivera (2002). A note on the dynamic and static discplacements from a point source in multilayered media, *Geophys. J. Int.* **148,** 619–627.

Manuscript received 11 May 2020
Published online 30 September 2020